3rd AIAA Atmospheric Space Environments Conference
27 - 30 June 2011, Honolulu, Hawaii

AIAA 2011-3376

Potential to reduce the climate impact of aviation by flight level changes

Ulrich Schumann,[1] Kaspar Graf,[2] and Hermann Mannstein [3]
Deutsches Zentrum für Luft- und Raumfahrt (DLR), Institut für Physik der Atmosphäre, 82230 Oberpfaffenhofen, Germany

Aircraft contribute to global and regional climate changes by contrail formation and by emissions of carbon dioxide and others species. Among these, contrails are considered to have the largest warming contribution on short time scales (up to order of decades) while carbon dioxide may cause the largest warming effect globally at long time scales (order of a century). Contrails warm generally during night. During day contrails may cause a cooling. This paper discusses various strategies to reduce the global warming from aircraft by contrail formation and carbon dioxide emissions. In particular, we discuss the impact of changes of the flight level, typically 2000 ft (610 m) up or down. Previous studies suggested reducing contrail formation by flying lower generally or by flying higher or lower at the actual level with minimum relative humidity. This paper introduces a more efficient strategy which selects optimized routes based on the climate impact of contrails and fuel consumption along these routes. By preferred flights in atmospheric regions where contrails cool, an aircraft routing can be designed with minimum or even negative climate impact. For the fleet as a whole the climate impact is measured in terms of its radiative forcing *RF*. For individual flights, the climate impact is measured by the amount of energy induced into the Earth-atmosphere system per unit flight distance, which we call the energy forcing *EF*. Both *RF* and *EF* for contrails and CO_2 can be combined into a global mean surface temperature increase for a given time horizon. This paper describes the basic principles and quantifies the potential impacts using the recently developed Contrail Cirrus Simulation Prediction tool (CoCiP).

Nomenclature

A	=	area, m^2
dt,ds	=	time step, distance step, s, m
C	=	coefficient
D	=	drag, N
EF	=	energy forcing, J m^{-1} or GJ km^{-1}
F	=	thrust, N
f	=	fuel flow per unit distance, kg m^{-1}
h	=	height, m or ft = 0.3048 m
H	=	time horizon of climate impact, a
LW	=	longwave contribution
M	=	Mach number
net	=	net value
RH_i	=	relative humidity over ice
RF	=	radiative forcing, W m^{-2}
s	=	length coordinate along flight path, m
S	=	wing area, m^2
SW	=	shortwave contribution

[1] Director of the DLR-Institute of Atmospheric Physics, Münchner Str. 20, 82230 Oberpfaffenhofen, Germany, and AIAA associate member.
[2] Doctoral Student.
[3] Scientist.

t = time, s
T = temperature, K
V_{TAS} = true air speed, m s^{-1}
W = contrail width, m
ρ = air density, kg m^{-3}

I. Introduction

AVIATION impacts climate by gaseous and particulate emissions. Besides carbon dioxide (CO_2), also nitrogen oxides, water vapor, soot and others contribute to the climate impact by aviation [1-4]. Among the various effects of aviation on climate, contrails are expected to cause the largest contribution to global radiative forcing of the Earth-atmosphere system, and hence the largest contribution to aviation–induced global climate change [5-9]. In air masses, which are cold enough as measured by the Schmidt-Appleman criterion [10], the water vapor emissions lead to local liquid saturation in the engine exhaust plume so that contrails form. In ambient humid air masses, with relative humidity above or near ice saturation [11], these contrails are long-lasting and may develop into cirrus clouds. High supersaturation with respect to ice is often found in the upper troposphere [12, 13]. The air mass layers with high supersaturation are often rather thin [14] so that rather small altitude changes may bring aircraft into drier layers where either less contrails or less persisting contrails form.

This paper discusses strategies to reduce the climate impact of aircraft by contrails and carbon dioxide. Various strategies have been suggested to avoid contrails, including vertical and horizontal route deviations to avoid contrail formation [15-18]. A previous study suggested reducing contrail formation by flying lower generally [19]. However, quite large flight level reductions of about 6000 ft (2 km) are needed to avoid about half of all contrails in the annual mean by such a strategy [20]. Similar contrail formation reductions can be achieved by smaller and only local flight level changes depending on the actual vertical profile of relative humidity [21], however this method does not guarantee minimum climate impact. These ideas may be used in conjunction with horizontal route optimization schemes [15-18, 22]. In this paper, we introduce a concept of climate optimized routing based on the local climate impact of these routes. The concept is illustrated with flight level changes, typically 2000 ft (610 m) up or down.

Climate optimizing of aircraft routes requires a suitable tool to compute the climate impact of the contrails and a conversion into a metric that allows for the comparison to the impact of additional fuel consumption caused by the deviation from a fuel optimized route. Such a tool and a suitable metric are described in this paper.

II. Optimization concept

Contrails and thin cirrus in general warm the Earth atmosphere by reducing terrestrial (longwave, LW) radiation loss into space and may cool the Earth atmosphere by reflecting part of the solar (short-wave, SW) radiation back to space [23-25]. During night, contrails are always warming. The largest climate impact by contrails comes from thick, wide, long and long-lasting contrails. Hence, with respect to climate, optimal routes during night are those which form contrails with minimum longwave warming. During day time, contrails may cool. This may be the case for thick contrails, over dark and cool surfaces, in particular in the morning and evening times when cirrus is more reflective than during mid day [24]. Hence, with respect to minimum contrail warming impact, optimal routes may be those causing contrails with maximum shortwave cooling.

CO_2 has a far longer residence time than all other aviation emissions [26]. For steady traffic emissions, and even more for a situation with decreasing emissions, the climate impact of CO_2 emissions dominates that of any short-term effect after some time (order decades). For growing traffic, above a critical growth rate depending on the radiative forcing and residence time ratios, the short-lasting contributions dominate the long-lasting CO_2 contribution during the time period with growing traffic emissions [27]. Any case, the fuel consumption has to be considered together with the contrails in climate optimal route optimization.

The potential for changes in climate impact by route changes depends on the sensitivity of the climate impact to geographical location and altitude and its variability for different weather conditions. When considering annual mean values, the changes in radiative forcing by flight level changes may be small. For example, a reduction of mean flight levels by an order 1 km causes about 10 % less ozone formation in the annul mean [28]. A change of flight levels by 2000 ft up or down changes the radiative forcing by linear contrails by about +5 % and -20 % [20]. On average flying lower reduces contrails in low latitudes and enhances the cover at high latitudes and vice versa [29]. Other studies show similar magnitudes [30, 31]. However larger variability can be expected with position and time for individual routes and route alternatives for different weather situations. Though we cannot show this formally, we expect that this variability is higher for contrails than for all other aviation climate effects, for reasons discussed next.

For CO_2, it is well known that the climate impact is, to good approximation, independent of the place and daytime of its emission. This is because CO_2 warms the lower atmosphere over its full residence time in the atmosphere, and this residence time is of order many decades. The residence time is far larger than the time required to mix CO_2 from a local place of emission over the whole atmosphere. In contrast, persistent contrails are formed in only 10-15% of the total flight distance and are short-lasting (order minutes to a day), so that their contribution to climate impact is rather local and depends strongly on the flight path and the weather situation there. For other emissions, the residence times are in between those for contrails and CO_2. For nitrogen oxides (NO_x), e.g., the upper troposphere residence time is of the order of a week and the ozone formed from NO_x has additional life times of order a several week [3]. For soot, the residence times may reach several weeks. Methane reductions from enhanced oxidation due to increased nitrogen oxide concentrations act on time scales of months to about a decade and are in between the short-lasting contributions and CO_2 therefore. Hence, we expect that the variability of *RF* relative to the mean value for fixed altitudes is far larger for contrails than for other emissions. Therefore contrails offer the largest chance to reduce the climate impact by aviation by small changes in routing (altitude, horizontal route, timing). Certainly, this conjecture should be studied for all aviation effects quantitatively in the future.

The contrail contribution to radiative forcing is very sensitive to various contrail parameters including thickness, temperature, time of day etc. [24]. Because of the large life-time of contrails, contrails formed late during day may start cooling but become warming when persisting after sunset. Early morning contrails may warm before sunrise but cool thereafter.

Contrail formation is obviously weather dependent. For optimal flight planning, one needs to know the weather of the coming day or days. Hence the optimization requires weather forecast data as input.

Contrail formation is aircraft dependent. Besides the obvious impact of flight altitude, speed and fuel consumption, the emission indices of water vapor (constant for the standard fuel: kerosene) and soot control the initial contrail ice formation [32]. The mass, speed and wing span of the aircraft determine properties of the wake vortices behind the aircraft and hence the initial contrail mixing and vertical displacement with possible loss of ice particles in the vortex regime [33, 34]. In order to be effective, route optimization should be performed preferably on long-distance routes with heavy aircraft (causing most of fuel consumption).

Contrail formation is obviously traffic dependent. Hence, one needs to know the traffic for past analysis and the demand for transport and type of aircraft as to be used in the coming days. The traffic information should provide the aircraft/engine type, the aircraft mass and speed, and the precise routing along waypoints from departure to destination airports.

The climate impact of contrails cannot be accurately computed from local variables along the flight route. Contrail formation and contrail persistence can be assessed from local meteorology and aircraft parameters. However the width, thickness, and length of the contrail, and its radiative properties are complex functions of the meteorology in the contrail neighborhood during the time span between contrail formation and contrail dissipation. Most previous models, as recently reviewed by Burkhardt et al. [35] and Frömming et al. [36], attempted to relate contrail properties to the ambient meteorology and to simple fleet parameters (such as distance flown or fuel consumed). They use a scaling to line-shaped contrail observations and hence do not account for details of contrail dynamics such as contrail advection, spread and dissipation. As a consequence they are unable to predict the impact of various aircraft properties. A first attempt to include contrail dynamics into a general circulation model have been reported by Burkhardt and Kärcher [9]. This model was successful in computing the cover and radiative forcing from contrail cirrus. But the method models contrails as subgrid-scale clouds and is designed for a fleet of aircraft and not for single flights.

Many aircraft flights contribute to contrails and climate. A considerable fraction of the 80000 flights of aircraft operating daily world wide, including the smaller business jets, reaches cold and humid air masses at altitudes where contrails form. All these flights may be included in a climate mitigation system.

This requires efficient and accurate computation tools. Several large-eddy simulation models have been developed (e.g., [34, 37, 38]) to simulate the wake vortex dynamics and the contrail cloud microphysics in detail. However, a prediction tool dealing with thousands of flights and many alternative routes during optimization, must provide a balance between accuracy and overall computational efficiency. The model presented below was designed with this purpose in mind.

Any deviation from a cost optimized route may cause considerable costs to the airline operator (fuel consumption, flight time, air traffic management, personnel) [19]. Also flying at lower altitude or inside clouds may encounter more turbulence and cause stress to the aircraft structure and discomfort to the passengers. On the other hand, flying higher may cause more structural loads by under-pressure, more cosmic radiation to the crew, and reduced safety limits with respect to the flight envelope. Therefore, route optimization will be realized only when proper incentives are given. Even then, the optimization tool must be accurate enough so that the costs of

unnecessary route deviations remain smaller than the equivalent "costs" of the reduced climate impact. These topics call for further investigations beyond the present paper.

III. The Contrail Cirrus Prediction Tool CoCiP

A. Overview

The "Contrail Cirrus Prediction Tool" (CoCiP) has been developed to compute the contrail properties for any individual aircraft flying along any given route, defined by a sequence of waypoints versus flight time, from one airport to another [39]. Here we give a short description of the model used.

The method uses numerical weather prediction (NWP) data to determine the meteorological conditions along the flight route and for the resultant contrails. Such data are provided by NWP centers both for analysis of past and as forecasts for the next few coming days. The model simulates contrails as occurring along waypoint sequences of aircraft routes. For each flight segment on which the Schmidt-Appleman criterion [10] is satisfied (regardless of whether persistent or not), the model initiates a contrail segment. The meteorological input needed for these calculations are computed by bilinear interpolation in the NWP fields for the given positions and times. The model then simulates the advection of the end points of the contrail segments with the ambient wind (vertical and horizontal) using a second order Runge-Kutta scheme. The model computes the number of ice particles and the mass of ice water per contrail length and assumes that the volume concentration of these parameters in the plane perpendicular to the plume axis can be approximated with a Gaussian distribution [40, 41]. The initial number of ice particles is a function of the number of soot particles emitted and initial dilution during the early wake vortex phase. The ice water content inside the contrail is computed assuming local equilibrium with respect to ice saturation. Later, the plume cross-section increases due to wind shear and vertical and lateral turbulent diffusion following analytical relationships [42]. The ice content changes with time according to mixing of the water vapor content in the plume with humidity from the ambient air, assuming that the humidity inside the plume stays ice-saturated. The number of ice particles per unit distance remains constant except for parameterized aggregation, turbulent particle loss, and sedimentation effects. Locally, the code computes the optical depth of the contrail segment as a function of the number concentration and ice water content and geometrical depth of the contrail plume, including a correction factor for the ratio between volume mean and effective radius [43]. This simulation is performed until the contrail becomes optically very thin (solar optical depth below 10^{-4}). This determines the maximum age t_{age} of the contrail segment. As a result CoCiP computes a sequence of way points with contrail segments in between. Usually the flight results into more than one consecutive set of contrail segments which are interrupted by contrail-free plume segments. In the analysis, each consecutive sequence of contrail segments is counted as one contrail.

From the model results, for each contrail segment, the radiative forcing (RF_{SW}, RF_{LW} and $RF_{nets} = RF_{SW}+RF_{LW}$) of the segment is estimated using efficient approximate functions derived by Schumann et al. [44]. These functions compute the *RF* induced as a disturbance to the fluxes at top of the atmosphere as a function of the radiative fluxes without contrails (as available from the NWP input) and as a function of the given contrail segment properties (solar optical depth, effective particle radius, temperature, cirrus cover above the contrail). Fit parameters in these functions have been calibrated with detailed radiative transfer model calculations with the libRadtran code [45] assuming contrails to be similar to plane cirrus clouds.

So far, CoCiP simulates the individual contrails individually and without feedback among each other or with the background meteorology. (This will be overcome in the next CoCiP version in which CoCiP gets integrated into a climate model.) Hence, the optical depth and *RF* values of a set of overlapping contrails is assumed to be equal to the sum of the individual contrail contributions. However, for analysis of contrail/cirrus cover, we account for overlap between individual contrails with background cirrus clouds. The sum of contrails and cirrus is seen as a representation of contrail cirrus. We define cloud cover as the area fraction of the superposition of contrails and cirrus clouds with total vertical solar optical depth larger than a critical value, here 0.05. For numerical evaluation we use a longitude-latitude grid with 5000×3000 grid cells in longitude×latitude around the equator and from pole to pole. For each grid cell we sum up the optical depth of the cirrus (computed from ice water content, effective radius, cloud cover fraction based on the NWP results) and the optical depth contributions from all contrails, assuming Gaussian spatial distributions as functions of the distance between contrail center line and the center point of the grid cells. The contrail-cirrus cover is determined on this grid as the difference of cloud cover with contrails minus that without contrails.

The model contains various model parameters which are adjusted so that the model results are consistent with various observations. Most critical are: 1) the number of ice particles assumed to be forming from the emitted soot particles and surviving the vortex phase, 2) the effective vertical velocity shear at contrail scale derived from the NWP data on rather coarse grids, and 3) the parameters determining maximum age of the contrails (ambient

humidity, turbulent mixing, aggregation of ice particles, sedimentation). Presently, the soot emission index value is set to a constant value 3.57×10^{14} kg^{-1} in this study, in rough agreement with previous estimates [46-48]. So far, the model has been tested in a few studies, and this process is ongoing. The tests performed so far include comparison to in-situ observations in young contrails [49] and comparison with METEOSAT-SEVIRI satellite observations of the diurnal cycle of cirrus in correlation with air traffic over the North Atlantic [39, 50]. Further tests are underway and may lead to further changes. Hence, the quantitative model results presented here are preliminary.

CoCiP is run either in a " *time-slice modus*" or a "*flight modus*". The first represents an *Eulerian* view to the contrails from the flights occurring before and until a given slice time; the second represents a *Lagrangian* view to the contrails from individual flights.

For analysis of the contrail and cirrus properties at given times, CoCiP is operated in the *time-slice modus*. Here, the code loops over a set of analysis time slices, typically with 1 h intervals, for the full year, i.e. 8760 time slices. For each time slice t, the simulation loops over all flights occurring in the time period (t-t_{age}, t) before this time, depending on a prescribed maximum contrail age t_{age} (6 or 24 h). All contrails surviving from formation until the time of analysis are included in the output results. This mode of analysis provides results which are comparable to satellite observations taken at the given time t.

For analysis of individual flights, CoCiP is run in the flight modus. In this modus, CoCiP performs a loop over all flights, including all waypoints from departure to destination, but, to save some computation time, presently only at flight levels above 150 hft. For each waypoint in time and space, CoCiP initiates a contrail segment which is followed in Lagrangian sense until the contrail in this segment disappears or until a selected maximum age t_{age} is reached.

For analysis of *EF* and *RF*, CoCiP contains a subroutine, which computes the contrail properties for a single flight over the life-cycle of the contrail. This routine steps from contrail formation until the end of the considered contrail period, in finite time steps of typically 1 h. The code needs access to the 3d meteorological fields from NWP for all times covering the life-cycle of the contrail. In the time-slice modus, this includes the times before the time of analysis covering the given maximum contrail age. In the flight modus, this includes the times from the first flight segment until the time of the last flight segment plus the given maximum contrail age.

The CoCiP model has been tested so far with various meteorological analysis data. The NWP model must be able to predict the relative humidity of the air including ice supersaturation properly. Here we use analysis data from the Integrated Forecast System (IFS) of the European Center for Medium Range Weather Forecasts (ECMWF) which has been demonstrated useful for this purpose [51-53]. In this study we use the data at 1° horizontal resolution, with 15 grid levels from about 4 to 15 km altitude (100 to 650 hPa), for the full year of 2006, every 3 h. The data are based on forecast results starting from analysis at either 00 or 12 UTC the same day with 6-15 h forecast times. The minimum forecast times of 6 h was found to be sufficient for relaxation of relative humidity from the assimilation process [51, 53].

Ice supersaturated layers may be very shallow requiring high vertical resolution. Short-term variability with small-scale vertical motions may contribute to contrail formation and dissipation. Hence, future studies have still to show whether the resolution used in this study is sufficient for accurate predictions. However, when we find a significant potential to reduce contrails in a coarse resolution simulation we may expect that the mitigation effects could be even larger if higher resolution input becomes available.

CoCiP may be run with various sources of traffic data. CoCiP has been tested first with waypoints generated to represent city pairs as provided by the Official Airline Guide (OAG), a commercial product including all traffic connections for scheduled traffic world wide in a certain period. We also run CoCiP with artificial test flights. For the analysis of the contrail impact of the presently operating fleet of aircraft, we use traffic data from the global ACCRI waypoint data set for 2006, as provided by Volpe, the FAA, and EUROCONTROL within the project ACCRI (see [54, 55]). These data provide waypoint coordinates (aircraft type, time, latitude, longitude, altitude, mass, fuel consumption, true air speed) for all commercial flight trajectories in the year 2006, about 80000 flights per day. These data are given with different segment lengths; they are homogenized by interpolation to 3 min segment duration or typically 42 km segment length, defining the minimum contrail length. Shorter segments would require more computer time but have only small impact on the global mean results.

B. Results: Annual mean contrail properties

Here we present a few selected results on annual mean contrail properties for meteorology of the year 2006 and for the ACCRI traffic data set of 2006, as obtained in the *time-slice modus*. The mean values are averages of the global contrail distributions as computed hourly for all days of the year.

The code is run with maximum contrail age t_{age} of either 6 or 24 h. Global and annual mean values are listed in Table 1. On average 4300 contrails (from one or several consecutive flight segments) are present at any time. The

global mean cirrus cover with optical depth larger 0.1, derived from the NWP data, is about 20 %. The contrail cover is about a factor of 100 smaller and amounts to about 0.22 % globally. This value is more than a factor of 2 larger than previous estimates for line-shaped contrails [36, 56]. The mean optical depth is near 0.1, but local values reach up to 2, in agreement with other studies [11, 57]. Many of the contrails form in subsaturated air masses and are short lasting therefore. Only about one third of the contrails form in supersaturated air masses in which they persist and grow to large widths. We note that the persistent contrails last for several hours, and reach quite large length and width values. These results appear not unrealistic [58], but case-by-case comparisons of computed contrail cover scenes with high-resolution satellite observations have still to be performed.

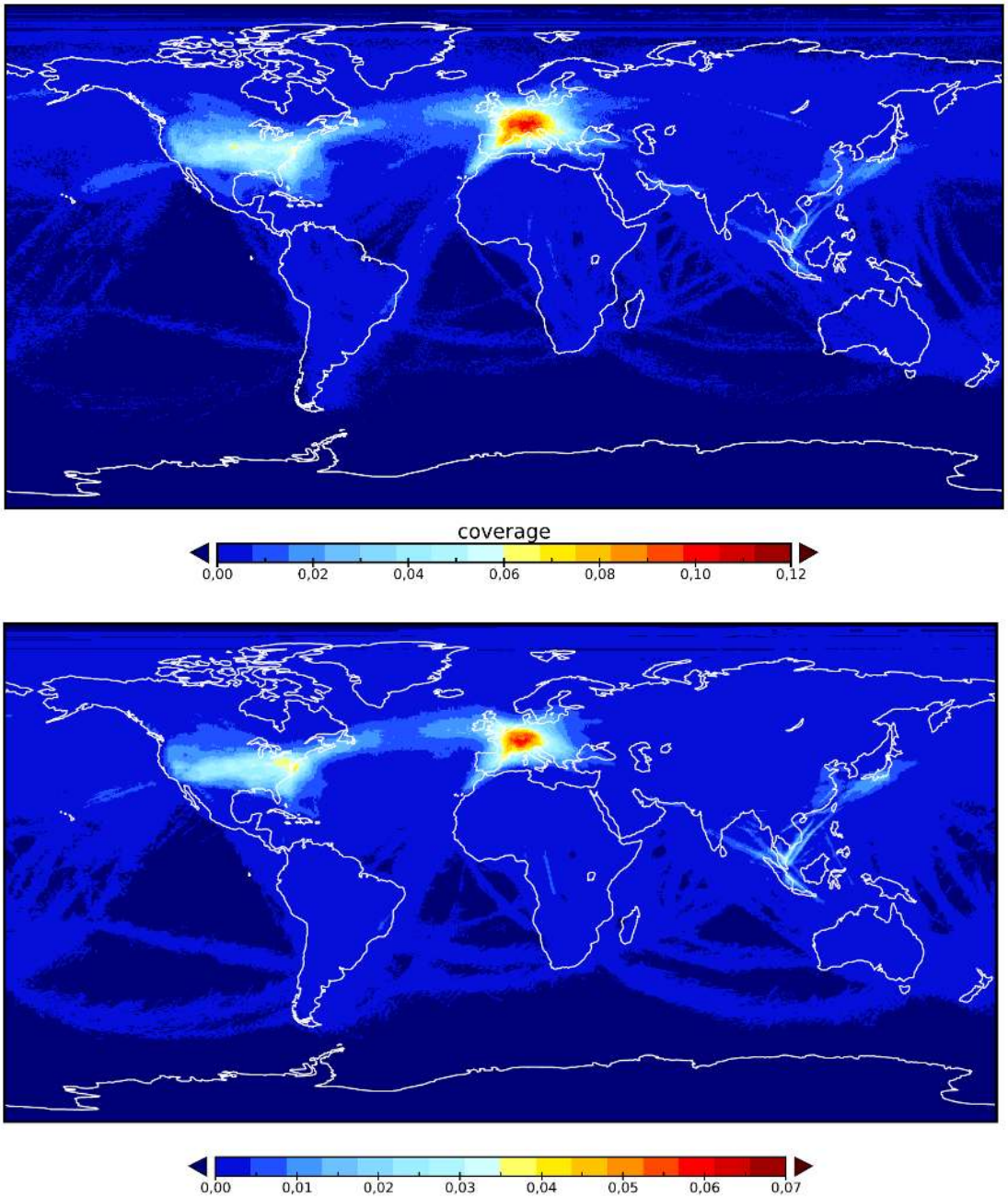

Figure 1. Annual mean contrail distribution. *Top: Annual mean additional cirrus cover with solar optical depth > 0.05 due to contrails. Bottom: Annual mean solar optical depth of the sum of contrails computed with CoCiP for the year 2006,* $t_{age} \leq 6h$.

The global mean value of radiative forcing *RF* in this case is 38 mW m^{-2} for 6 h maximum contrail age and about 50 mW m^{-2} for 24 h maximum contrail age in this CoCiP simulation. The details depend on several CoCiP model parameters so that these results should not be taken as final. Based on various parameter studies and preliminary comparisons to observations, we estimate the best estimate *RF* value for global contrail induced cirrus cover in the range 25 to 90 mW m^{-2}. This range is consistent with other estimates [8, 9].

Figure 1 shows the mean contrail cover and the mean solar optical depth. Both have a similar distribution. As expected the contrail cover is largest and optically thickest over Europe and the Eastern USA. One may note the diffuse appearance of contrails in terms of optical depth (with low cover) along the routes flown rarely over the Southern Pacific and Indian Ocean. This reflects lateral transport of contrails away from the routes with wind.

Table 1: Annual mean contrail properties for the global fleet of commercial aircraft in 2006

Parameter and mean values:	$t_{age} < 6$ h	$t_{age} < 24$ h
Mean traffic density (above 150 hft)	0.0074 km^{-1} h^{-1}	same
Mean fuel consumption per distance flown	4.75 kg km^{-1}	same
Fraction of flight distance with contrail formation	0.39	0.39
Fraction of flight distance in ice supersaturated air	0.14	0.18
Number of flights causing contrails at a time	3350	3770
Number of consecutive contrail segments at a time	4300	4960
Contrail contribution to global cirrus cover	0.22 %	0.29 %
Length of contrails	410 km	396 km
Width of contrails	5.7 km	6.4 km
Age of contrails	2.3 h	2.7 h
Number of ice crystals per length in fresh contrails	1.5×10^{12} m^{-1}	1.4×10^{12} m^{-1}
Number of ice crystals per length at analysis time	0.9×10^{12} m^{-1}	0.88×10^{12} m^{-1}
Solar optical depth	0.091	0.093
Fraction of contrails forming inside thin cirrus	93 %	92 %
Optical depth inside cirrus	0.13	0.13
Optical depth outside cirrus	0.08	0.09
Contrail radiative forcing, longwave RF_{LW}	0.093 W m^{-2}	0.118 W m^{-2}
Contrail radiative forcing, shortwave RF_{SW}	-0.057 W m^{-2}	-0.069 W m^{-2}
Contrail radiative forcing, net RF_{Net}	0.037 W m^{-2}	0.049 W m^{-2}

IV. Climate impact metric: Radiative forcing and energy forcing

Traditionally, one assesses the climate impact of a disturbance to the climate system in terms of its instantaneous radiative forcing *RF*. Here we define *RF* as the global mean amount of energy flux change at top of the atmosphere[4] per time unit and area unit of the Earth surface. *RF* reflects an Eulerian view of the system at a given time. *RF* can be estimated from the sum of *RF* values of all individual contrails at a given time *t*

$$RF_{net}(t) = \frac{1}{A_{Earth}} \sum_{flights} \int_{length} RF_{nets}(t,s)\, W(t,s)\, ds\,. \tag{1}$$

Here A_{Earth} is the Earth surface area, and $RF_{nets}(t, s) = RF_{LW}+RF_{SW}$ is the net radiative forcing from longwave and shortwave contributions (W m^{-2}) for a contrail segment of geometrical width $W(t, s)$ at a certain position *s* along the contrail at time *t*.

This *RF* describes the net effect of flights at a given time, it does not describe the net effect for an individual flight (in a Lagrangian sense) over the life-cycle of the contrails (and other emissions). For example, at the time *t* of this analysis, an individual contrail may have just formed, with small width and little radiative forcing. Its major effect may come later when it has spread and grown by uptake of water from ambient air. This may not matter if we compute *RF* for a large fleet of aircraft or average over many times, but this *RF* will characterize the fleet as a whole

[4] The IPCC definition of RF with respect to flux changes at the tropopause is more difficult to implement because it requires computation of the thermal adjustment of the stratosphere to an instantaneous disturbance.

and not the individual flights. Of course one can optimize the fleet climate impact or the impact of a type of aircraft flying regularly by minimizing *RF*, but one cannot optimize an individual flight between given city-pairs with this concept.

For individual flights, we assess the climate impact of the disturbance induced by the flight to the climate system in terms of the amount of energy per flight distance, which we call "energy forcing" *EF*. As for the instantaneous *RF*, we compute the *EF* response at top of the atmosphere without climate feedbacks. Here we use a Lagrangian view and follow the climate impact along the flight path. The climate impact is measured in terms of the integral energy input over the lifetime of the contrail per flight distance,

$$EF = \int_{lifetime} \left(RF_{nets}(t',s)\, W(t',s) \right) dt' \tag{2}$$

Here *EF* is the amount of energy per unit flight distance for a single flight (in units of J m^{-1}) induced into the atmosphere system without feedback on the atmosphere because of instantaneous net radiative forcing $RF_{nets}=RF_{LW}+RF_{SW}$ from longwave and shortwave contributions (W m^{-2}) on average over the contrail width *W* (m) per unit length of the flight segment, from time $t'= t$ of contrail formation until contrail disappearance at $t=t+ t_{age}$, with increment *dt'*(s).

For typical values [24], RF_{nets}= 10 W m^{-2}, width *W*=1000 m, and contrail life time 10000 s, we expect a mean value of *EF* ~ *RF*×width×lifetime. This product is of order 100 GJ km^{-1} per contrail length. The value per unit flight distance is about a factor of ten smaller because radiatively important contrails form only on about 10 % of all flight segments.

The two concepts, based on *RF* or *EF*, are quite different and we could not find an explicit relationship between them. However, we may consider the global energy input *E* by contrails over the time t_{year} = *1 a* of a year. This energy can be computed both from *EF* and *RF*. The energy *E* equals the integral of the mean energy input per unit flight distance, *EF*, or approximately its annual mean value <*EF*> times the total flight distance, L_{tot}, in the sum over all flights per year. It also equals the annual mean radiative forcing <*RF*> times the Earth surface A_{Earth} and the period of a year t_{year}:

$$E=\langle RF \rangle A_{Earth}\, t_{year} = \sum\nolimits_{flights} \int_{length} EF(t,s)\, ds \cong \langle EF \rangle L_{tot}\,, \quad L_{tot} = \sum_{flights} \int_{length} ds\,. \tag{3}$$

Hence,

$$\langle EF \rangle \cong \frac{t_{year}\, A_{Earth}}{L_{tot}} \langle RF_{net} \rangle\,. \tag{4}$$

This approximation provides a lower bound only, since longer contrails provide larger *EF* values and this correlation is ignored in the last part of Eq. (3). For a mean fuel consumption of about 5 kg km^{-1} (Table 1) and a total global aviation fuel consumption of about 200 Tg a^{-1} [2], the total flight distance per year is $L_{tot}=40\times10^{12}$ m a^{-1}. The Earth surface is $A_{Earth}= 4\pi R^2$, *R*= 6371 km. For RF_{net} of e.g. 30 mW m^{-2}, which is the expected magnitude for aviation induced cloudiness [3, 9], we obtain a mean value *EF*= 12 GJ km^{-1}. The magnitude of this estimate is consistent with our previous estimate (10 GJ km^{-1}).

In principle, the *EF* and *RF* metrics differ also for CO_2 emission. However, for CO_2, one usually ignores the details of the mixing processes in the individual plumes and instead assumes immediate mixing over the whole atmosphere, because the mixing occurs at a time scale far shorter than CO_2 life time.

V. Estimate of additional fuel consumption

Besides contrails, the CO_2 from burning kerosene is another main driver of climate change. Hence, in order to assess the impact of flight level changes, we have to consider both the changes in contrails and in fuel consumption. The computation of fuel consumption for aircraft is a standard task, but requires aircraft/engine specific input not readily available for climate studies. Therefore, we present the computation of fuel flows here in some detail.

The fuel consumption *f* (in kg m^{-1}) of an aircraft is computed from its aerodynamic drag *D* which determines the necessary equivalent thrust *F*. The drag and thrust values are functions of the aircraft/engine types, and of true air speed V_{TAS}, aircraft mass *m*, altitude *h*, and ambient temperature *T*. They can be computed for individual aircraft with given engine types using input, e.g., from the performance tables of the EUROCONTROL Experimental Centre base of aircraft data (BADA) [59]. Basically, one computes the drag

$$D = \frac{C_D \rho V_{TAS}^2 S}{2} \tag{5}$$

(Eqs. 3.6-1-3.6-4 of BADA) for given speed V_{TAS} , air density ρ and wing area *S*. Since the drag equals thrust for steady cruise, *f* is computed from

$$f = C_{fl}\left(1 + \frac{V_{TAS}}{C_{f2}}\right) C_{fcr} D \tag{6}$$

(Eqs. 3.9-1 to 3.9-7 of BADA).

The maximum cruise altitude is given by the condition that the drag stays below the maximum cruise thrust $(F_{cruise})_{MAX}$ provided by the engine as required for minimum speed. The maximum cruise thrust is slightly smaller than the maximum climb thrust, $(F_{cruise})_{MAX} = C_{Fcr} \times (F_{max})_{cl}$, $C_{Fcr} = 0.95$. Hence, the maximum cruise altitude *h* is constrained by

$$D = \leq C_{Fcr}(F_{\max})_{cl}\,,\ (F_{\max})_{cl\,ISA} = C_{Tc1} \times \left(1 - \frac{h}{C_{Tc2}} + C_{Tc3} h^2\right) \tag{7}$$

under international standard atmosphere (ISA) conditions (Eqs. 3.7-1 to 3.7-8 of BADA). Here, the aircraft/engine type specific parameters *S*, C_D, C_{fl}, C_{f2}, C_{fcr} C_{Tc1}, C_{Tc2}, C_{Tc3} are taken from the performance tables provided in the BADA data bank. For non-ISA conditions, the maximum climb thrust $(F_{max})_{climb}$ changes as a function of the deviation from the standard atmosphere temperature and further aircraft type specific coefficients.

We have evaluated these data for all aircraft types encountered in real air traffic in 2006 and 2008, as far as available in the BADA files. Here we show results on fuel consumption for flight altitudes *h* above 270 hft (8230 m), assuming flights in an ISA-atmosphere [59]. The true air speed is computed for BADA-given cruise Mach number *M* as a function of the speed of sound $V_{TAS} = M\sqrt{\gamma RT}$, with isentropic expansion coefficient (γ=1.4 for air), and universal gas constant *R*= 287.04 J (kg K)$^{-1}$, and altitude-dependent temperature *T*. The aircraft mass *m* is either taken as the operational reference mass or the maximum mass.

Figure 2 shows the fuel consumption as computed this way for various aircraft/engine types, from a small business jet Falcon 20 (FA20) to a heavy wide-body jet aircraft of type Airbus A380-800 (A388). We see, that the fuel consumption increases and the maximum cruise flight level decreases with aircraft mass. Somewhat higher flight levels can be reached with increasing fuel consumption for lower speed, above the buffeting limit, or for

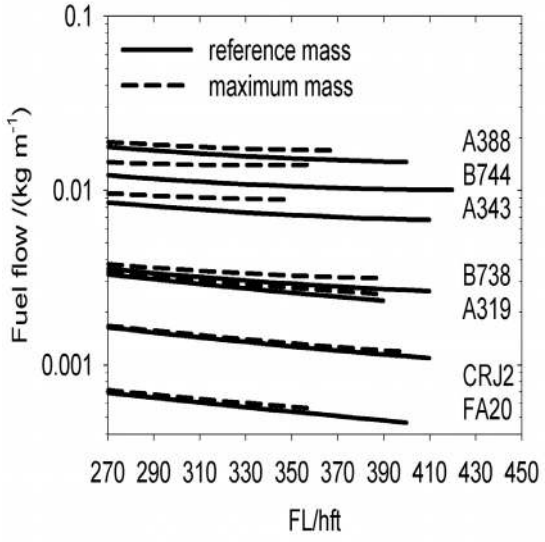

Figure 2. Fuel consumption *f* versus flight level. *Fuel consumption per unit flight distance as a function of altitude h (flight level FL) for a set of aircraft types, selected for illustration, for ISA atmosphere, fixed cruise Mach numbers, and either the reference mass or maximum mass of aircraft, using BADA 3.7 data.*

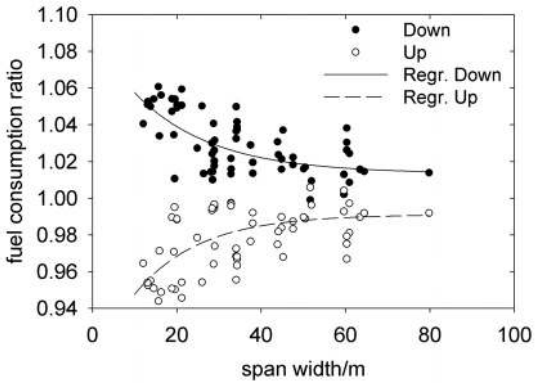

Figure 3. Fuel consumption ratio versus aircraft span width. *The ratio is the fuel consumption per flight distance in air at a flight level 2000 ft up or down relative to a reference flight level (10000 m or about 330 hft). The symbols denote the results for aircraft reaching these flight levels for ISA atmosphere, fixed cruise Mach numbers, and reference mass of aircraft, using BADA 3.7 data. The regression curves are used for rough interpolation.*

reduced mass. However, here we consider only fixed cruise Mach numbers and fixed mass. For this case, with the operational reference mass, the fuel consumption per unit distance decreases with flight altitude for most jet aircraft in operation and the operation mass. For higher aircraft mass, the minimum fuel consumption may arise at lower flight levels.

The ratio of fuel consumption at a higher or lower flight level (2000 ft up or down) relative to the fuel consumption at a reference flight level has been computed this way for the ISA atmosphere, fixed reference aircraft mass, and fixed Mach number. As can be deduced from the steepness of the curves in Fig. 2, the ratio decrease with aircraft mass. The correlation of this ratio with aircraft mass for different aircraft types is weak. A slightly better correlation is found when plotting this ratio versus aircraft span width, see Fig. 3. This plot applies to a reference altitude of 10000 m (about FL 330 hft). The regression curves are $ratio_{down}(s) = 1.013+0.07582\times\exp(-0.05427\times s)$, and $ratio_{up}(s) = 0.9911-0.08356\times\exp(-0.06507\times s)$, where s = span width in m. Hence, flying 2000 ft higher (lower), if possible, generally reduces (increases) the fuel consumption by up to 1 to 6 %, decreasing with aircraft size (mass and span).

The computed changes are roughly consistent with the literature. For example, Döpelheuer and Lecht [60] find that the fuel consumption for various aircraft engine combinations decreases with increasing altitude. For 1000 ft higher flight levels, they computed a decrease of fuel consumption of about 1.5 to 2 % for a B747-400, MD11, and DC10-30, increasing with decreasing aircraft masses. Williams et al. [19] also use the BADA data and report an increase in fuel consumption when reducing flight levels of the airliner fleet generally. Fichter et al. [20] find a fuel consumption increase (decrease) by 2.7 % (-0.5%) for a general flight level reduction (increase) of 2000 ft when possible in a global emission data base (TRADEOFF). Similarly Grewe et al. [28] and Gauss et al. [61] report a 5.8 % and 5.1 %, respectively, increase in global fuel consumption for a 6000 ft downward shift of flight altitudes under cruise conditions.

In the present study the additional fuel consumption for step climbs and descents is ignored and assumed to be small compared to the total amount of additional fuel consumption required to fly higher or lower. This may be overcome in future applications. Döpelheuer and Lecht [60] have computed the additional fuel consumption for a step climb for one aircraft on a long-distance flight. The increase in fuel flow rate is a few percent of the normal rate and the time period of such steps is short compared to the total cruise time, at least for long-distance flights with a small number of additional steps.

VI. Global warming trade offs

The gain in climate protection by reducing warming contrails by flight level changes has to be paid with possibly increased fuel consumption and related carbon dioxide emissions from aviation (besides cost effects). This is true in particular when flying lower than optimal. Here we investigate the climate contribution of contrails and CO_2 from aircraft and ask for the critical limit in fuel consumption below which contrail reduction is useful for long-term climate protection. Other items of trade-offs like increased air traffic management or operation costs are beyond the range of this study.

As metric for long-term climate impact we use the absolute global temperature potential AGTP(H) for a selectable time horizon H, typically 50 and 100 years [26]. Here AGTP is the global mean surface temperature increase ΔT due to a unit disturbance. For CO_2 the disturbance is the unit mass of fuel burned per flight distance. For contrails, the disturbance is the unit amount of energy induced by contrails per flight distance. The AGTP for CO_2 assumes immediate mixing of the emitted CO_2 gas amount over the Earth atmosphere and a gradual uptake of CO_2 by the biosphere and the ocean. The resultant concentration increase of CO_2 causes an additional energy input to the Earth-atmosphere system. Likewise, contrails cause a local energy input to the earth atmosphere system. We assume that the localized energy input has the same climate impact as a globally distributed energy input. The energy input increases the global mean surface temperature depending on the heat capacity of the atmosphere. This increase decays with time because of radiative loss to space and energy uptake by the ocean. These effects are described by equations given in Fuglestvedt et al. (2010) [26], and we coded them in Fortran, see appendix. Their Eqs. (A2, A3) for a CO_2 pulse are similar to those given by Sausen and Schumann [62], but differ in the thermal inertia model. Fuglestvedt et al. use a two-term instead of one-term representation. For sustained emissions (at a rate constant with time and an amount equal to the pulse amount), the AGTP is the time integral of the pulse AGTP over time until time horizon H divided by H.

As mentioned, we assume that the local energy input by individual contrails has the same effect as the globally distributed energy input resulting from uniform CO_2 concentration increase. The ratio between the global temperature increase for a local energy input relative to that for a CO_2-equivalent globally distributed energy input is called efficacy factor. For the annual mean contrail cover, an efficacy factors of about 0.6 has been determined by

Ponater et al. [63, 64]. The energy efficacy factor for individual contrails has still to be determined. Here we assume simply an efficacy factor of one. For a smaller efficacy, the impact of individual contrails on global climate change would be correspondingly smaller.

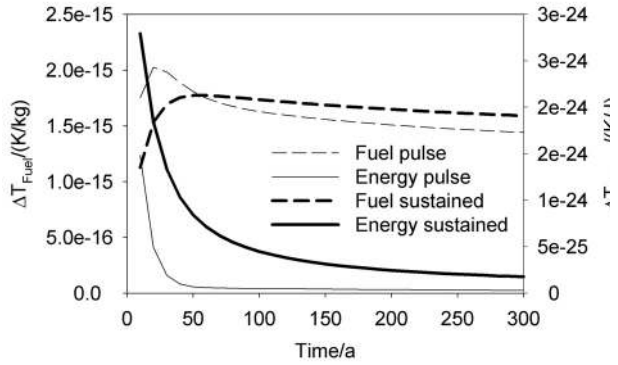

Figure 4. Absolute global temperature potential. *Global mean surface temperature increase due to carbon dioxide emission from carbon dioxide from kerosene (EI_{CO2} = 3.15 kg/kg) per unit fuel mass (kg) burnt (thin curves) and due to energy from contrails induced into the atmosphere per unit energy (J) input (thick curves), for a pulse emission (dashed curves) or for constant sustained emission (full curves), as a function of time horizon.*

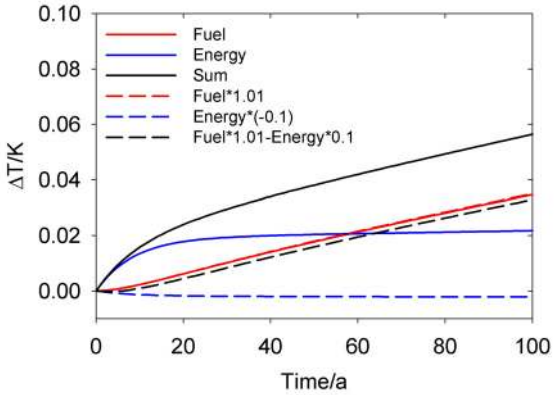

Figure 5. Scenarios of fuel and energy contributions to global mean temperature. *Full curves for the reference scenario and dashed curves for a scenario with increased fuel consumption and negative energy input versus time horizon. For details of the scenarios see the text.*

Figure 4 shows the AGTP for pulse and for sustained consumption of fuel and for a pulse and sustained input of energy per unit flight distance, with efficacy of one, as computed this manner. For fuel, the initial increase of the temperature response is caused by the gradual increase of energy captured by the greenhouse effect of CO_2 and its decay due to thermal inertia. After a maximum response of the temperature (after about 20 years for a pulse and 40 years for sustained emissions) it again decreases because more and more of the CO_2 gets lost from the atmosphere. The asymptotic effect at large times stays finite because a finite amount (21.7 %) of the initially emitted CO_2 remaining in the atmosphere in this model. The maximum of temperature response is reached later and the temperature decreases slower later in the sustained compared to the pulse case because the emissions occur later. Note that the response is computed for unit emissions, which means that the emissions per year decrease with increasing time horizon H for the sustained mode. For a unit energy input at time zero (pulse) or uniformly distributed over the time H, the temperature increase is largest initially because later part of the heat gets lost to the ocean or to space. After H=50 a, the values reached are

$$\Delta T = 1.81\times10^{-15}\ \mathrm{K\ kg^{-1}},\ 6.98\times10^{-26}\ \mathrm{K\ J^{-1}},\ 1.77\times10^{-15}\ \mathrm{K\ kg^{-1}},\ 8.44\times10^{-25}\ \mathrm{K\ J^{-1}}$$

for fuel and energy, pulse or sustained, respectively.

The same response function can be used to assess the temperature increase for a given radiative forcing of contrails with an equivalent energy input $E = RF\ A_{Earth}\ H$, see Eq. (3) (Earth surface in m^2 and time horizon H =1 a). For example, for RF = 30 mW m^{-2} in the sustained mode, the temperature response after 50 years is 0.0203 K.

Figure 5 shows the temperature increase due to aviation CO_2 emissions in two scenarios. In the reference case (full curves) the assumed fuel consumption is 200 Tg per year and the energy input from short lasting forcing such as contrails corresponds to a radiative forcing of 30 mW m^{-2}, both in sustained mode. In the changed scenario (dashed curves) the fuel consumption is increased by 1 %, and the energy input is assumed to be negative and 10 % of the original value in magnitude. The results show that the negative energy input balances the total CO_2 induced warming for the first 6 years in this case. Later, the total temperature increase in the scenario with reduced energy input stays significantly below the reference result, in spite of the 1 % increase in fuel consumption, for more than 300 years. This period is finite because of the finite amount of CO_2 remaining in the atmosphere for infinite times in this model. Nevertheless, in this example, the reduced energy input (ΔEF = 1.1 EF in this case) balances the increased fuel consumption (Δf = 0.01 f) for centuries.

Obviously, there exists a critical value Δf_{crit} of additional fuel consumption which can be balanced by the reduced energy input ΔEF. Formally the critical values Δf_{crit} follows from

$$\Delta f_{crit}\ \Delta T_{fuel}\ (H) = \Delta EF\ \Delta T_{energy}(\mathrm{H}). \qquad (8)$$

The value Δf_{crit} (not plotted) depends strongly on ΔEF, time H, and the scenario mode. The value of Δf_{crit} generally decreases with time horizon H. It decreases most quickly for a pulse emission. It is larger for a sustained mode and largest for scenarios with large prescribed annual percentage increase rates of growing traffic. Hence, a reduction of contrails pays off in a climate sense for only a limited time horizon if done once or for a short period (pulse) but pays off far longer and possibly for unlimited times if introduced in a sustained mode or in a scenario with growing air traffic.

VII. Air traffic with climate optimized flight levels

A. Optimized flight levels example – Lagrangian view on one flight

In this section we report results of route optimization for a single flight based on CoCiP running in the Lagrangian flight modus as explained above using energy forcing as metric. Here, CoCiP is applied five times, (1) for a reference case in which all flights occur at the original flight levels. Thereafter, CoCiP is applied after shifting all flight levels (2) 2000 ft up or (3) 2000 ft down uniformly over the whole flight, or (4), for each contrail segment, after shifting it 2000 ft up or down to the level with lowest relative humidity, or (5), for each contrail segment, shifting it 2000 ft up or down to the level with lowest energy forcing. Note the last version requires to first simulate the full life-cycle of the contrail for each contrail segment at each of the three alternative levels from contrail formation until the contrails die out. The results are used to compute the energy forcing by integrating the local *RF* values times contrail width over the segment length and the full life-cycle of the contrail segments. At the end the contrail properties are computed again for the sequence of flight segments at the optimal flight levels.

Figure 6 shows an example for an individual flight which should illustrate how the method works. Reduced energy forcing is achieved by either avoiding contrails or by stronger SW forcing. The example demonstrates that contrails may cause a cooling when selecting proper flight levels.

In this example, a B747-400 left Amsterdam (AMS) at about 1150 UTC 6 June 2006 and arrived in San Francisco (SFR) about 9.5 h later. The route along the waypoints (above 150 hft) is 8550 km long. The *EF* analysis was performed allowing for up to 24 h contrail age, but the maximum age stayed below 9.4 h in this case. Flight level changes by ±2000 ft were introduced, without checking the maximum thrust condition, Eq. (7), at the higher levels.

The top panel of Fig. 6 shows the westbound flight route, approximately following a great circle connection. The air temperature (T_{air}, shown for the reference case only) was partially above, partially below the Schmidt-Appleman threshold temperature T_{SAC} for contrail formation. Over large parts of the flight, over the North Atlantic, the air was too warm and too dry to let contrails form. The second panel shows the flight altitudes flown. The black curve is the reference altitude. The recorded flight data as used for the reference case show that the aircraft performed two step climbs during this flight, the first near 15°W, the second near 86°W. The fuel flow rate logged for this case in the ACCRI data set does not show any significant increase of the fuel flow rate during these step climbs.

The blue curve depicts the altitude for the case when the route was optimized to fly at minimum relative humidity over ice (RHi). In this optimization, flight level changes were activated only when the ambient humidity was above 90 %, i.e. when persistent contrails were expected to form. Hence, in the third panel the blue curve equals the minimum value of the RHi encountered for RHi>0.9. We see that in this case the aircraft had to fly higher or lower, with 12 additional steps up or down in between, partly switching between the lowest and the highest flight levels.

The red curve shows the flight levels for the flight with minimum energy forcing per unit distance *EF*. For this example, flight level changes are activated only when the reduction in energy forcing by such level changes exceeds 20 GJ/km. This extra condition avoids unnecessary flight level changes with only minor gain in energy forcing. Because of this extra condition, the selected flight level (red curve) remained high over the North Atlantic when no contrails formed. Otherwise, the optimized route often follows the min-RHi route, but not always. Over the whole flight, the *EF*-minimum required 10 additional FL changes in this case.

The panel above the lowest panel shows the energy forcing computed for this flight. The *EF* values are zero when flying without contrails (because of low humidity or high ambient temperature). Short contrails cause very small *EF* values. For the early and final parts of the route, at high ambient humidity, and partly within optically thin cirrus clouds, the individual *EF* values are very large, reaching up to 3500 GJ km^{-1} in the reference case, because of wide, thick and long-lasting contrails. The *EF* values are positive for most part of the route indicating warming contrails. The min-RHi variant provides *EF* values which are lower than the *EF* for the reference case mostly, but not always. In fact, near 15°W, the min-RHi case gives larger *EF* values than the reference case in this example.

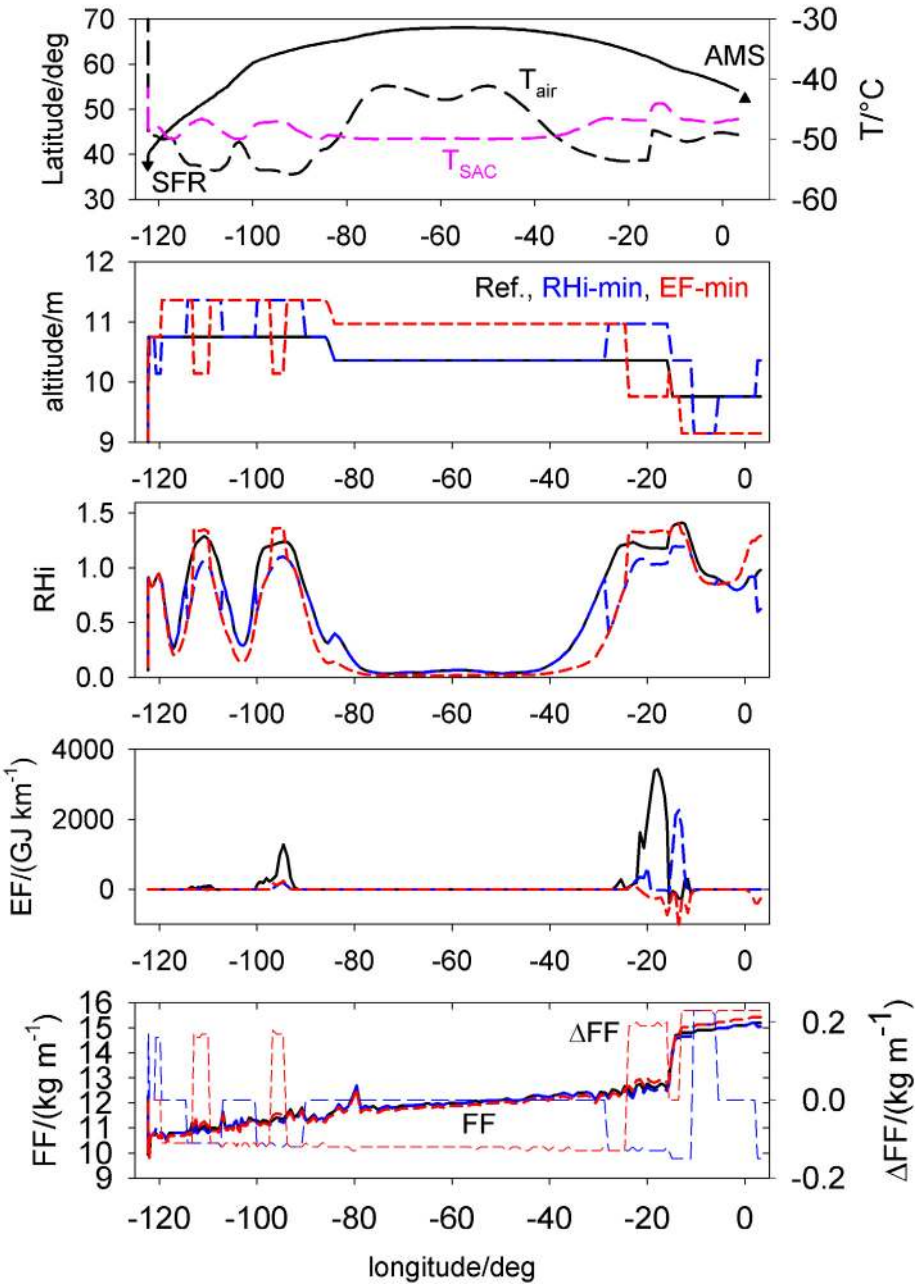

Figure 6. Flight level optimization example. *Results for a flight of a B747 from Amsterdam-Schiphol AMS to San Francisco SFR, with route map (triangular symbols denote airport locations), flight altitudes, air temperature (T_{air}, dashed blue), and Schmidt-Appleman threshold temperature (T_{SAC}, dashed purple), relative humidity over ice (RHi), energy forcing per meter (EF), fuel consumption FF per meter (full) and change in fuel consumption per meter ΔFF (dashed), along the flight route versus longitude, for three strategies: black: reference; blue minimum RHi; red: minimum EF.*

Finally, the lowest panel shows the fuel consumption FF per unit distance. The black curve for the reference case depicts the ACCRI data. We see that the fuel consumption was large initially, and decreased with time, in particular after the first step climb near 16°W. The changed values of FF for varied flight level (red and blue) are hardly discernable in the scales. Therefore, the changes ΔFF required for changed flight levels are plotted in separate scales. The changes amount to about 1 % of the fuel flow FF in the reference case, with positive values for flying lower.

The min-*EF* variant, however, gives the lowest *EF* values always, by definition. This flight is an example with large positive *EF* values in the reference case and negative mean value *EF* in the optimized case. In the *EF*-optimized case, the *EF* values are mostly zero (no contrails). In the eastern part of the flight leg, at noon time, the *EF* values for the optimized flight levels are negative. Here, the contrails are cooling. Cooling contrails are reached mainly by flying a little lower, in the upper troposphere with high ambient humidity.

Table 2 summarizes mean values for this example flight. The units may require explanations: 1 Mg = 10^6 g = 1000 kg, 1 TJ = 10^{12} J, 1 GJ = 10^9 J, 1 nK = 10^{-9} K. In this example, we have a double gain: First, the amount of fuel required for *EF*-minimum is slightly smaller than in the reference case, because of the large fraction of upward flight level changes (still to be checked for feasibility). Second, the contrail energy induced changed from positive to negative.

The global mean surface temperature increase resulting from this example flight are listed in Table 2. The temperature changes are simply the products of the response functions for pulse responses shown in Fig. 4 with the fuel and energy amounts for this flight as given in Table 2. Table 2 shows the temperature changes for H=50 years. For other time horizons, the changes can be deduced from Fig. 4. (In a future CoCiP version we plan to minimize the climate impact not in terms of *EF* but in terms of the sum of temperature increases due to the segment specific fuel consumption and contrail energy, for given time horizon H.)

Consequently, the global mean surface temperature change induced by this flight, for a time horizon of 50 years, in the sum of contrail and CO_2 effects, is about a factor of two smaller in the *EF* case than in the reference case. The other strategies give results in between the reference case and the *EF*-minimum case for this flight. We see that this single flight, acting as pulse emission, causes a warming also in the EF-optimized case. If such flight level optimization would be performed daily in a sustained mode, the procedure could contribute to global cooling, with contrail cooling compensating the CO_2 warming for the total fuel consumption of such flights.

Table 2: Flight mean values for the example flight for various flight level optimization strategies. *F: fuel burned, E: energy induced by contrails, FF: mean fuel flow rate, EF: mean energy forcing, T: temperature increase after 50 years from CO_2 of fuel burned, from contrail induced energy, and from the sum of both.*

Strategy	F	E	FF	EF	T_{Fuel}	T_{Energy}	T_{sum}
unit	Mg	TJ	kg km^{-1}	GJ km^{-1}	nK	nK	nK
reference	103.6	1284	12.13	150.3	0.187	0.090	0.277
2000 ft up	102.6	575	12.00	67.2	0.185	0.040	0.226
2000 ft down	105.2	-64	12.31	-7.5	0.190	-0.004	0.186
Min RHi	103.4	455	12.10	53.3	0.187	0.032	0.219
Min EF	103.5	-273	12.11	-31.9	0.187	-0.019	0.168

B. Optimized flight levels for the global air traffic

For illustration of the differences between *EF* optimization and *RF* optimization we first show results for *RF* optimization. Hence, in this section we report results of route optimization for a fleet of aircraft flights at a sequence of times based on CoCiP running in the Eulerian time-slice modus as explained above using radiative forcing as metric. Here, CoCiP is again applied five times, first (1) for a reference case in which all flights occur at the original flight levels. Thereafter, CoCiP is applied after shifting all flight levels (2) 2000 ft up or (3) 2000 ft down uniformly, or after (4) shifting it 2000 ft up or down to the level with lowest relative humidity, or (5) shifting it 2000 ft up or down to the level with lowest radiative forcing at the time of analysis. Again, the last version requires to first simulate the contrail over its life-cycle from contrail formation until the time of analysis for each contrail segment at each of the three alternative levels. The results are used to compute the radiative forcing by averaging the local *RF* values times contrail width over the segment length at the time of analysis. At the end, the contrail properties are computed again for the sequence of flight segments at the optimal flight levels.

Figure 7 shows *RF* values for a set of flights on one day (6 June 2006). The contrails occurred at altitudes between 7.5 km and 12.5 km in this situation, as expected for the bulk of air traffic. At lower altitudes contrails may not form because it was too warm. At higher levels contrails may not form because the atmosphere was too dry. We find warming contrail contributions from LW forcing and cooling contributions from SW forcing. The local net values are either positive or negative. The left hand panel shows the results for the reference case. The right hand panel shows the result after flight level optimization for minimum radiative forcing *RF*. We see that in the minimum

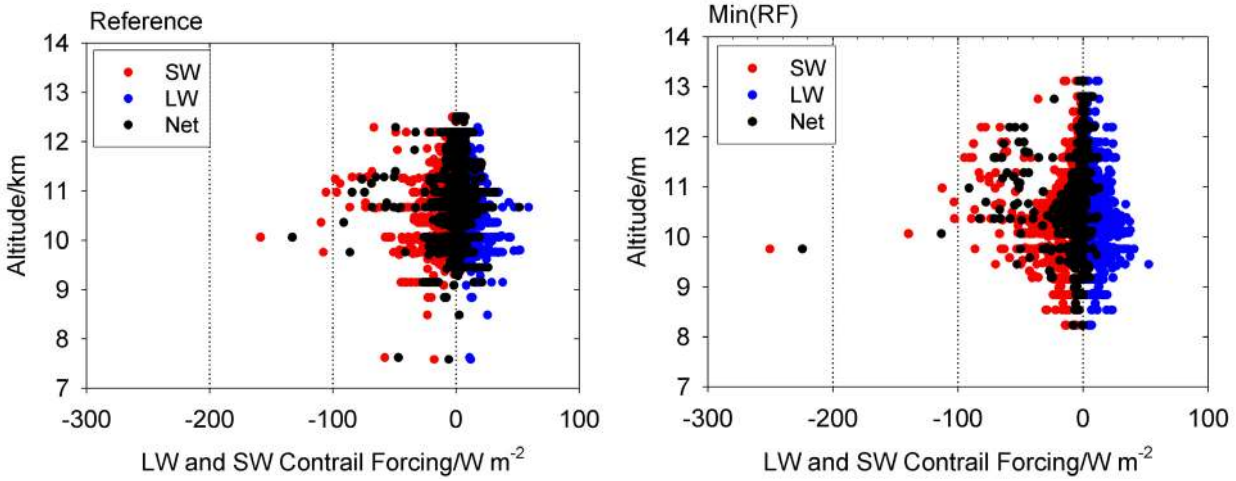

Figure 7. Radiative forcing by contrail segments versus altitude without and with RF optimization. *Shortwave (SW), longwave (LW) and net radiative forcing (RF, Net) values at contrail segments versus flight altitude for a small subset of flights at four selected times 0, 6, 12, 18 UTC 6 June 2006. Left: reference case. Right: after flight level changes to minimum RF. Note the bulk of the black symbols (net RF) shifts further left for the Min(RF) case and includes higher flight levels.*

Table 3: Annual mean radiative forcing for the 2006 aircraft fleet with various flight level optimizations. *Global and regional mean values of the radiative forcing (RF) in W m^{-2}, and related statistic; net, LW, SW: net, longwave, shortwave contribution, for $t_{age} \leq 6$ h.*

Strategy	Reference	higher	lower	Min RHi	Min RF
net global	0.037	0.035	0.034	0.017	-0.0044
LW global	0.094	0.085	0.090	0.043	0.058
SW global	-0.057	-0.050	-0.056	-0.026	-0.062
Net relative	*100.0 %*	*94.6 %*	*91.9 %*	*45.9 %*	*-12.0 %*
Fuel/(kg/km)	4.75				
ΔFuel/(kg/km)	0	-0.157	0.390	-0.0212	0.0054
Contrails km/km	0.394	0.468	0.309	0.349	0.386
ISSR km/km	0.182	0.122	0.154	0.091	0.178
net USA	0.278	0.257	0.245	0.131	-0.020
LW USA	0.742	0.662	0.685	0.345	0.483
SW USA	-0.464	-0.405	-0.440	-0.214	-0.532
Net USA relative	*100.0 %*	*92.4 %*	*88.1 %*	*47.1 %*	*-7.2 %*
net EUR-M	0.691	0.494	0.795	0.302	-0.041
LW EURM	2.023	1.420	2.363	0.877	1.345
SW EURM	-1.331	-0.926	-1.568	-0.576	-1.460
Net EUR-M relative	*100.0 %*	*71.8 %*	*115.6 %*	*43.9 %*	*-6.0 %*

RF case, the net *RF* values are generally shifted to smaller or more negative values, as intended. The differences give some impression of how the method works. The reduced radiative forcing is achieved by either avoiding contrails, or causing contrails with shorter lifetimes, or by stronger SW forcing.

Though the quantitative values depend on the specific day and traffic selected, and may change depending on details of the CoCiP model, this shows the reduction potential. Further gain can be expected by varying the flight route horizontally or by changes in departure times.

On average over all hourly time steps within a full year, Table 3 gives some statistics of contrail properties and radiative forcing for the globe and for two subregions; USA: 130°W – 65°W, 25°N-55°N, also considered by Palikonda et al., 2005 [65]; and EUR-M: 10°W – 20°E, 40°N – 55°N, see Meyer et al., 2000, 2007 [66, 67]. The mean values are averages over the full year of results computed in 1 h intervals. Here, CoCiP is applied with maximum contrail age of 6 h.

By variation of the flight levels by ±2000 ft, the climate impact measured in *RF* can be reduced globally, see Table 3. The *net relative percentage* values show the relative impact of the various mitigation strategies. Present aviation flies at an altitude where the global radiative forcing is close to a maximum, at least for this test case. Hence, flying higher everywhere or flying lower everywhere helps to reduce the contrail induced radiative forcing. However, flying higher does not pay off in the tropics or over mid-latitudes at summer times when the tropopause is higher than the flight altitudes.

About half of the globally integrated radiative forcing can be avoided when flying higher or lower depending on the local relative humidity. Flight changes are effective in particular at mid latitudes (such as over the USA, mid Europe, and North Atlantic) where flying higher implies flights in the lower (drier) stratosphere.

However, the results show that the contrail climate impact can be changed in sign, from warming to cooling when optimizing the flight levels according to the radiative forcing *RF* of the individual flight segments.

The results shows that the min-*RF*-strategy causes smallest *RF* globally but also in 18 other subregions analyzed (here shown for USA and Europe). Hence, route optimization is efficient both globally and regionally. On the other hand, the SW forcing is only a few percent more negative than the SW forcing in the reference case. Hence this strategy does not induce unacceptable cooling by contrails.

C. Optimized flight levels for all flights of the global airliner fleet

In this section we report results of applying CoCiP in the flight modus to all individual flights in the ACCRI waypoint data base and compute the *EF* value as defined above, as the integral of the local radiative forcing multiplied with contrail width over the flight path length and the contrail life time.

Figures 8 and 9 show the *EF* results for a subset of flights on one day (6 June 2006). The plots show the variability of *EF* versus altitude, relative humidity, contrail age, and fuel consumption. Note that this is the value of energy input from contrails per flight distance, including *EF*=0 locally for flight segments without contrails. The variability of *EF* is even larger than the high variability of *RF* shown before (Fig. 7). Individual values (up to 6000 GJ km^{-1}) can be more than 100 times larger than the mean value.

Figure 8 shows the *EF* results for the reference case (black) and for optimized flight levels which may be 2000 ft higher or lower depending on *EF* (red). The scatter of the values is far smaller in the optimized case compared to the reference case. We see that *EF* minimization is particular worthwhile in ice-supersaturated regions with moderately high ambient humidity. However the *EF* does not simply increase with increasing ice supersaturation, partly because high supersaturation causes large ice particles which sediment quickly and hence remain short-lasting. Figure 9 shows that *EF* is largest for contrails with long lifetimes, as expected, but the trend is hardly significant. Figure 9 also shows that *EF* is aircraft type dependent, as expected, but only moderately. *EF* is the larger the more fuel the aircraft consumes. However, the scatter induced by different meteorology is far larger than the variability due to different aircraft types.

The mean *EF* for the 2006 aircraft fleet is 62.9±17.3 GJ km^{-1} in our reference case with t_{age}= 6 h, see Table 4. The range given reflects the standard deviation of 122 individual 3-days mean values relative to the annual mean value. The large variability causes some statistical uncertainty. Obviously, one year of data is just sufficient for significant *EF* averages.

After route optimization for minimum *EF* relative to ±2000 ft flight levels changes, the mean fleet energy forcing decreases close to zero, see Table 4. For the reference case, the fleet mean fuel consumption is about 4.6 kg km^{-1}. For *EF*-optimized routes, the additional fuel consumption required to fly at higher or lower flight levels is 0.0093 ± 0.0040 kg km^{-1} on average. Hence, the mean additional fuel consumption amounts to only 0.1 % of the total mean fuel consumption. This small value is a consequence of the fact that flights are nearly as often shifted to higher flight levels as to lower ones, with opposite signs of additional fuel consumptions. Moreover, only 12 % of all flights occur in ice supersaturated air masses. Hence flight level changes are needed only rarely.

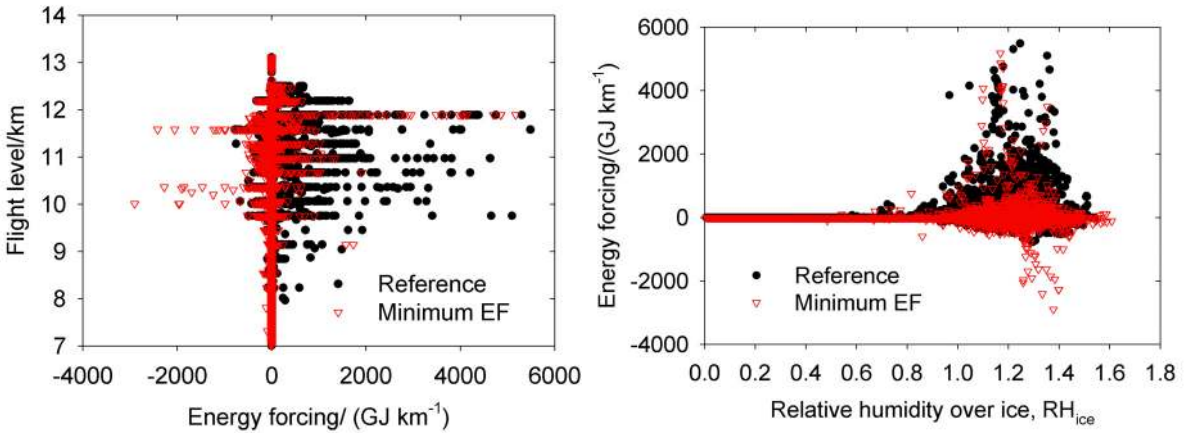

Figure 8. Energy forcing EF without and with EF optimization. *Left: Energy forcing EF versus flight level altitude for the reference case (black) and for a minimum EF optimization (red) for individual contrail segments of a small subset of flights on 6 June 2006. Right: same versus relative humidity over ice at time of contrail formation.*

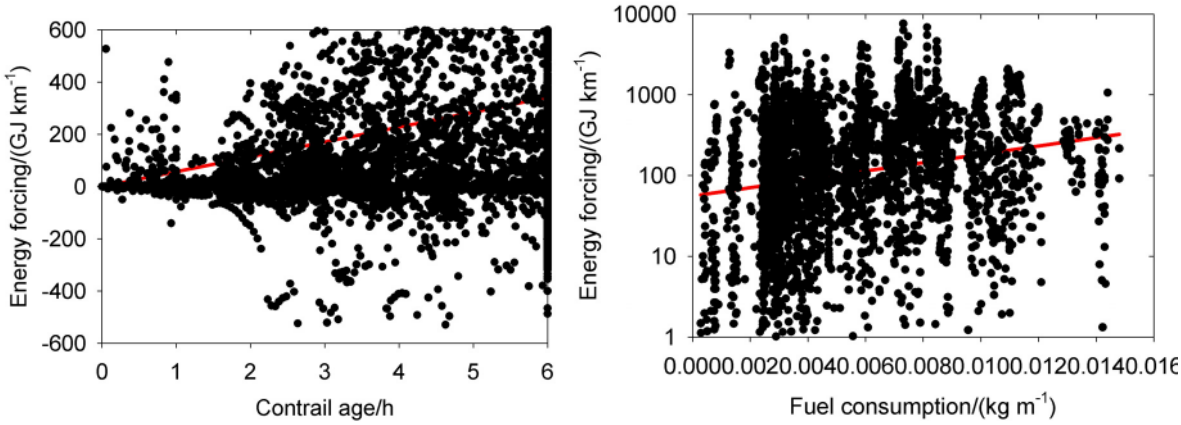

Figure 9. Energy forcing EF as a function of contrail age and fuel consumption. *Left: Energy forcing EF versus maximum age of the contrail segments for the reference case for individual contrail segments of a small subset of flights on 6 June 2006. The plot shows the results within ±600 GJ km^{-1}. The mean regression (red line) increases from 0 to about 340 GJ km^{-1} for contrail ages from 0 to 6 h. Right: Energy forcing (positive values only, in logarithmic scales) versus fuel consumption of the contrail generating aircraft. The regression line (red, based on the log-scale EF values) shows an increase of EF with fuel consumption.*

Table 4: Annual mean values of energy forcing and fuel consumption for 2006 traffic in the flight modus

Parameter	Reference flight levels	Minimum EF flight levels
Mean Energy forcing, GJ km^{-1}	24.5±6.7	0.8±1.6
Mean fuel consumption, kg km^{-1}	4.64	
Mean additional fuel consumption, kg km^{-1}	0	0.0093 ± 0.0040

VIII. Conclusion

In conclusion, we have described a concept to optimize air traffic such that the combined climate effect of contrails and fuel consumption of aircraft can be minimized either flight by flight or for the fleet of aircraft in operation at given times as a whole. Routing can be optimized, depending on the actual or predicted weather conditions, such that the contrail impact gets reduced or even may become negative (cooling) instead of positive (warming) by avoiding the most warming contrails during night and by enhancing the most cooling contrails during day time. Since the warming by contrails is not a simple function of relative humidity, flights with minimum climate impact are different from flights avoiding persistent contrails by avoiding flights in ice supersaturated regions. Optimizing flight levels for minimum global warming is more efficient in reducing the climate impact than selecting flight levels with minimum relative humidity to avoid contrails. The concept is also far more efficient in respect to climate than requiring general reductions in flight levels. Flight level changes for optimal routes, upwards or downwards, are required only for a small part of the total flight distances. Higher flight levels, if possible, offer less fuel consumption. Typically 2000 ft (610 m) flight level changes up or down, are sufficient for strong reductions of the warming by contrails. The actual effects may be even larger than shown here when increasing vertical resolution in the NWP data, resolving very shallow ice supersaturated layers. The fuel flow penalty for this concept is small. The fuel consumption increases by a few percent for 2000 ft lower flight levels, and this value decreases with aircraft size. However, because flight level changes are required only rarely in this concept, the penalty is limited to about 0.1 % of the total fuel consumption on average over the fleet.

The reduced warming (or enhanced cooling) by contrails may balance at least part of the CO_2 induced warming by aviation, at least for some time. Negative energy input by contrails may overcompensate the warming by the CO_2 from the *total* fuel consumption for some years, but not far longer. However, even when the contrail warming stays positive, the reduced warming by contrails often exceeds the CO_2 warming due to the (small) *additional* fuel consumption for long time periods of the order of several centuries. The method is most efficient in protecting climate if applied in a sustained mode during times with growing air traffic.

For the climate impact of contrails from individual flights, from departure to destination, the proper metric for flight optimization is the amount of energy induced by contrails into the Earth-atmosphere system per unit flight distance, which we call the energy forcing *EF*. For a contrail at a given time, the common metric is the radiative forcing *RF*. Both concepts give results which are similar in a qualitative sense. Both give the same total energy input to the atmosphere on average over many flights and long times, but differ in detail. The *EF* is computed in a Lagrangian manner by integrating over the life-cycle of the contrails. The *RF* is computed in an Eulerian frame for contrails at a given time instant. The *EF* method should be superior to the *RF* method with respect to minimizing the climate impact of individual flights because it includes the warming induced by the contrails over their full life-cycle.

A contrail simulation tool CoCiP is described that has been developed to simulate the contrail dynamics after formation behind aircraft, flight by flight, globally for given meteorological fields (analysis or forecasts). CoCiP is a rather efficient tool for dealing with thousands of flights. Hence it may be implemented into commercial flight planning tools presently used to minimize airliner operation costs for given meteorology. CoCiP can be used to compute the *EF* or *RF* from contrails flight by flight.

Both, the *EF* and *RF* of contrails can be converted into an absolute global temperature potential (AGTP). The AGTP of contrail energy input can be combined with the AGTP of the radiative forcing from the related CO_2 emissions to make both comparable for given time horizons *H*.

CoCiP, just as all models, is based on simplifying assumptions and uses inputs with limited accuracy. Hence the model results have uncertainties. So far, the model has been tested in a few studies. Improvements are still possible and the quantitative model results may change. However, the principal result that flight routes may be optimized to produce minimum aviation climate impact should be robust.

In the future, the concept may be improved in various directions. Certainly, further validation and related improvements of CoCiP have a high priority. Detailed comparisons of computed contrail scenes with satellite observations, one-to one at given times, are ongoing. Higher resolution NWP forecast data may improve agreement with observations. CoCiP is presently being integrated into a climate model to quantify the impact of exchange of water vapor and soot between contrails and the background atmosphere. The change in fuel flow for changed flight levels as well as maximum cruise altitude should be computed explicitly for given aircraft type, mass, and ambient temperature. The optimization routine may avoid inefficient step changes (with small changes in *EF*) and minimize the global temperature change including the amount of fuel required for step changes. Studies of the impact of uncertainties on the prediction accuracy can be performed by proper parameter studies with the model. The concept

may be extended to reach even larger reductions of aviation climate impact by including variations in the horizontal routes. For this purpose, CoCiP may be used to compute EF for given aircraft types as a function of space and time and the routing may be designed to avoid regions with high EF. The method may also be used within schemes to optimize not only flights but the air transport system in a more general sense. It would be desirable to include the climate impact from other aviation effects besides contrails and CO_2, such as nitrogen oxides emissions. Studies of the practical consequences and costs of applying such models in real air traffic management systems and airline operations should follow. Finally, the necessary incentives required for acceptance of this method in spite of additional costs in support of climate protection for growing air traffic should be considered.

Appendix

The following Fortran-77 functions compute DTFUEL=ΔT_{Fuel} for 1 kg of fuel burned and DTENERGY= ΔT_{Energy} for 1 J of energy input as a function of time horizon H (in years) and for either IPULSE=1 (unit pulse emission) or 2 (constant or sustained emission). The theory follows Fuglestvedt et al. [26] as described above.

```
      FUNCTION DTFUEL(H,IPULSE)
c Temperature increase per kg kerosene fuel
c                                      pulse, K/kg
      REAL AJ(0:3)/0.217,0.259,0.338,0.186/
c               ! pulse response CO2
     $,ALPHAI(3)/172.9,18.51,1.186/ !
c       years of CO2 decay rate
     $,CJ(2)/0.631,0.429/ ! pulse response temperature
c                            ! K/(W m-2)
     $,DJ(2)/8.4,409.5/ ! years of temperature decay rate
     $,EICO2/3.15/ ! CO2_Emission-Index
c                             (kg CO2 per kg fuel)
     $,ACO2/1.82E-15/ ! specific radiative forcing
c                            per mass CO2
c H = Time horizon in years
      S1=0.
      S2=0.
      if(IPULSE.eq.1) THEN
c eq. (A3) of Fuglestvedt et al. (2010)
      DO J=1,2
      S1=S1+AJ(0)*CJ(J)*(1.-EXP(-H/DJ(J)))
      DO I=1,3
      S2=S2+
     1AJ(J)*(ALPHAI(I)*CJ(J)/(ALPHAI(I)-DJ(J)))
     2     *(exp(-H/ALPHAI(I))-EXP(-H/DJ(J)))
      END DO
      END DO
      ELSE
c (Integral over time H of ((eq. (A3))*dt)/ H
      DO J=1,2
      S1=S1+AJ(0)*CJ(J)*(1.-(DJ(J)/H)
     1 *(1.-EXP(-H/DJ(J))))
      DO I=1,3
      S2=S2+AJ(J)*(ALPHAI(I)*CJ(J)
     1 /(ALPHAI(I)-DJ(J)))
     2     *((ALPHAI(I)/H)*(1.-exp(-H/ALPHAI(I)))
     3       -(DJ(J)/H)*(1.-EXP(-H/DJ(J))))
      END DO
      END DO
      END IF
      DTFUEL=EICO2*ACO2*(S1+S2)
      RETURN
      END

      FUNCTION DTENERGY(H,IPULSE)
c temperature increase per unit energy pulse input, K/J
      REAL CJ(2)/0.631,0.429/ !
c               pulse temperature-response, K/(W m-2)
     $,DJ(2)/8.4,409.5/ ! years of temperature decay rate
     $,AE/6.21637E-23/ !
c  AE= 1./(4.*PI*(RADIUS**2)*24*3600*365)
     $ ! = 1./(Earth surface*time of year)
c H = Time horizon in years
c eq. (A2) of Fuglestvedt et al. (2010)
      S3=0.
      if(IPULSE.eq.1) THEN
      DO J=1,2
      S3=S3+CJ(J)*exp(-H/DJ(J))/DJ(J)
      END DO
      ELSE
c (Integral over time H of ((eq. (A2))*dt)/ H
      DO J=1,2
      S3=S3+CJ(J)*(1.-exp(-H/DJ(J)))/H
      END DO
      END IF
      DTENERGY=AE*S3
      RETURN
      END
```

Acknowledgments

This work contributes to the DLR project “Climate-compatible Air Transport System” (CATS). This works also was part of a project “Reduction of contrails by flight route optimization” (UFO) funded by the German Federal Ministry BMBF (Klimazwei). The results are contributions to the EU project “Reducing Emissions from Aviation by Changing Trajectories for the benefit of Climate” (REACT4C). The emissions inventories used for this work (cited as “ACCRI” data in the text) were provided by US DOT Volpe Center and are based on data provided by the US Federal Aviation Administration and EUROCONTROL in support of the objectives of the International Civil Aviation Organization Committee on Aviation Environmental Protection CO_2 Task Group. Any opinions, findings, and conclusions or recommendations expressed in this material are those of the authors and do not necessarily

reflect the views of the US DOT Volpe Center, the US FAA, EUROCONTROL or ICAO. This data set was provided to the authors within the Aviation Climate Change Research Initiative (ACCRI). The authors gratefully acknowledge cooperation with Pat Minnis and Joyce Penner within two ongoing ACCRI projects. Finally, we thank Simon Unterstrasser and Sigrun Matthes for suggestions which helped to improve this paper.

References

1. IPCC. *Aviation and the Global Atmosphere*. Cambridge, UK: Cambridge Univ. Press, 1999.
2. Lee, D. S., Fahey, D. W., Forster, P. M., Newton, P. J., Wit, R. C. N., Lim, L. L., Owen, B., and Sausen, R. "Aviation and global climate change in the 21st century," *Atmos. Env.* Vol. 43, No. 22-23, 2009, pp. 3520-3537, doi:10.1016/j.atmosenv.2009.04.024.
3. Lee, D. S., Pitari, G., Grewe, V., Gierens, K., Penner, J. E., Petzold, A., Prather, M. J., Schumann, U., Bais, A., Berntsen, T., Iachetti, D., Lim, L. L., and Sausen, R. "Transport impacts on atmosphere and climate: Aviation," *Atmos. Env.* Vol. 44, No. 37, 2010, pp. 4678-4734, doi:10.1016/j.atmosenv.2009.06.005.
4. Sausen, R., Isaksen, I., Hauglustaine, D., Grewe, V., Lee, D. S., Myhre, G., Köhler, M. O., Pitari, G., Schumann, U., Stordal, F., and Zerefos, C. "Aviation radiative forcing in 2000: An update on IPCC (1999)," *Meteorol. Z.* Vol. 14, 2005, pp. 555 - 561, 10.1127/0941-2948/2005/0049.
5. Minnis, P., Ayers, J. K., Palikonda, R., and Phan, D. "Contrails, cirrus trends, and climate," *J. Clim.* Vol. 17, 2004, pp. 1671-1685
6. Schumann, U. "Formation, properties and climate effects of contrails," *Compt. Rend. Phys.* Vol. 6, 2005, pp. 549 - 565
7. Mannstein, H., and Schumann, U. "Aircraft induced contrail cirrus over Europe," *Meteorol. Z.* Vol. 14, No. 4, 2005, pp. 549 - 554, 10.1127/0941-2948/2005/0058.
8. Stordal, F., Myhre, G., Stordal, E. J. G., Rossow, W. B., Lee, D. S., Arlander, W., and Svendby, T. "Is there a trend in cirrus cloud cover due to aircraft traffic?," *Atmos. Chem. Phys.* Vol. 5, 2005, pp. 2155-2162
9. Burkhardt, U., and Kärcher, B. "Global radiative forcing from contrail cirrus," *Nature Clim. Change* Vol. 1, 2011, pp. 54-58, DOI: 10.1038/NCLIMATE1068.
10. Schumann, U. "On conditions for contrail formation from aircraft exhausts," *Meteorol. Z.* Vol. 5, No. 1, 1996, pp. 4-23
11. Voigt, C., Schumann, U., Jessberger, P., Jurkat, T., Petzold, A., Gayet, J.-F., Krämer, M., Thornberry, T., and Fahey, D. W. "Extinction and optical depth of contrails," *Geophys. Res. Lett.* Vol. 38, No. 11, 2011, p. L11806 doi:10.1029/2011GL047189.
12. Gierens, K., Schumann, U., Helten, M., Smit, H., and Marenco, A. "A distribution law for relative humidity in the upper troposphere and lower stratosphere derived from three years of MOZAIC measurements," *Ann. Geophysicae* Vol. 17, 1999, pp. 1218 - 1226
13. Gettelman, A., Collins, W. D., Fetzer, E. J., Eldering, A., Irion, F. W., Duffy, P. B., and Bala, G. "Climatology of upper-tropospheric relative humidity from the Atmospheric Infrared Sounder and implications for climate," *J. Clim.* Vol. 19, No. December, 2006, pp. 6104-6121
14. Spichtinger, P., Gierens, K., Leiterer, U., and Dier, H. "Ice supersaturation in the tropopause region over Lindenberg, Germany," *Meteorol. Z.* Vol. 12, No. 3, 2003, pp. 143-156
15. Gierens, K., Lim, L., and Eleftheratos, K. "A review of various strategies for contrail avoidance," *Open Atmos. Sci. J.* Vol. 2, 2008, pp. 1-7
16. Campbell, S. E., Neogi, N. A., and Bragg, N. B. "An operational strategy for persistent contrail mitigation," *9th AIAA Aviation Technology, Integration, and Operations Conference (ATIO)*. Hilton Head, South Carolina, 2009, pp. 1-14.
17. Sridhar, B., Chen, N., and Ng, H. K. "Simulation and optimization methods for assessing the impact of aviation aperations on the environment," *27th Intern. Congress of the Aeronautical Sciences (ICAS2010)*. Nice, France, 2010, pp. 1-11.
18. Sridhar, B., Chen, N. Y., Ng, H. K., and Linke, F. "Design of aircraft trajectories based on trade-offs between emission sources," *9th USA/Europe Air Traffic Management Research and Development Seminar (ATM2011), http://www.atmseminar.org/*. Berlin, Germany, 2011.
19. Williams, V., Noland, R. B., and Toumi, R. "Reducing the climate change impacts of aviation by restricting cruise altitudes," *Transp. Res.* Vol. D7, 2002, pp. 451–464
20. Fichter, C., Marquart, S., Sausen, R., and Lee, D. S. "The impact of cruise altitude on contrails and related radiative forcing," *Meteorol. Z.* Vol. 14, No. 4, 2005, pp. 563-572, doi:10.1127/0941-2948/2005/0048
21. Mannstein, H., Spichtinger, P., and Gierens, K. "How to avoid contrail cirrus," *Transp. Res.* Vol. D 10, 2005, pp. 421–426
22. Sausen, R., Nodorp, D., and Land, C. "Towards an optimal flight routing with respect to minimal environmental impact," *Impact of Emissions from Aircraft and Spacecraft upon the Atmosphere. Proc. of an Intern. Sci. Colloquium, Köln (Cologne), Germany, April 18-20, 1994*. ISSN 0939-298X, Cologne, Germany, DLR Mitteilung 94-06, 1994, pp. 473-478.
23. Minnis, P., Schumann, U., Doelling, D. R., Gierens, K., and Fahey, D. W. "Global distribution of contrail radiative forcing," *Geophys. Res. Lett.* Vol. 26, No. 13, 1999, pp. 1853 - 1856

24. Meerkötter, R., Schumann, U., Minnis, P., Doelling, D. R., Nakajima, T., and Tsushima, Y. "Radiative forcing by contrails," *Ann. Geophysicae* Vol. 17, 1999, pp. 1080-1094, doi: 10.1007/s00585-999-1080-7.
25. Liou, K. N. "Influence of cirrus clouds on weather and climate processes: A global perspective," *Mon. Wea. Rev.* Vol. 114, 1986, pp. 1167-1199
26. Fuglestvedt, J. S., Shine, K. P., Berntsen, T., Cook, J., Lee, D. S., Stenke, A., Skeie, R. B., Velders, G. J. M., and Waitz, I. A. "Transport impacts on atmosphere and climate: Metrics," *Atmos. Env.* Vol. 44, No. 37, 2010, pp. 4648-4677, doi:10.1016/j.atmosenv.2009.04.044.
27. Grewe, V., and Stenke, A. "AirClim: an efficient tool for climate evaluation of aircraft technology," *Atmos. Chem. Phys.* Vol. 8, 2008, pp. 4621-4639, SRef-ID: 1680-7324/acp/2008-8-4621.
28. Grewe, V., Dameris, M., Fichter, C., and Lee, D. S. "Impact of aircraft NO_x emissions. Part 2: Effects of lowering the flight altitude," *Meteorol. Z.* Vol. 11, No. 3, 2002, pp. 197-205
29. Fichter, C. "Climate Impact of Air Traffic Emissions in Dependency of the Emission Location and Altitude," *DLR Forschungsbericht 2009-22, ISSN 1434-84543*. Oberpfaffenhofen, 2009, p. 152.
30. Koehler, I., Sausen, R., and Reinberger, R. "Contributions of aircraft emissions to the atmospheric NOx content," *Atmos. Env.* Vol. 31, No. 12, 1997, pp. 1801-1818
31. Rädel, G., and Shine, K. P. "Radiative forcing by persistent contrails and its dependence on cruise altitudes," *J. Geophys. Res.* Vol. 113, 2008, p. D07105, doi:10.1029/2007JD009117.
32. Kärcher, B., and Yu, F. "Role of aircraft soot emissions in contrail formation," *Geophys. Res. Lett.* Vol. 36, 2009, p. L01804, doi:10.1029/2008GL036649.
33. Sussmann, R., and Gierens, K. "Lidar and numerical studies on the different evolution of vortex pair and secondary wake in young contrails," *J. Geophys. Res.* Vol. 104, 1999, pp. 2131-2142
34. Lewellen, D. C., and Lewellen, W. S. "The effects of aircraft wake dynamics on contrail development," *J. Atmos. Sci.* Vol. 58, 2001, pp. 390-406
35. Burkhardt, U., and Kärcher, B. "Process-based simulation of contrail cirrus in a global climate model," *J. Geophys. Res.* Vol. 114, No. D16201, 2009, pp. 1-13, doi:10.1029/2008JD011491.
36. Frömming, C., Ponater, M., Burkhardt, U., Stenke, A., Pechtl, S., and Sausen, R. "Sensitivity of contrail coverage and contrail radiative forcing to selected key parameters," *Atmos. Env.* Vol. 45, 2011, pp. 1483-1490, doi:10.1016/j.atmosenv.2010.11.033.
37. Gierens, K. "Numerical simulations of persistent contrails," *J. Atmos. Sci.* Vol. 53, 1996, pp. 3333-3348
38. Unterstrasser, S., and Sölch, I. "Study of contrail microphysics in the vortex phase with a Lagrangian particle tracking model," *Atmos. Chem. Phys.* Vol. 10, 2010, pp. 10003–10015, doi:10.5194/acp-10-10003-2010.
39. Schumann, U. "A contrail cirrus prediction tool," *Proceedings of the 2nd International Conference on Transport, Atmosphere and Climate (TAC-2). 22-25 June 2009, DLR-Forschungsbericht 2010-10, Köln-Porz, Germany, ISSN 1434-8454*. Aachen, Germany, and Maastricht, The Netherlands, 2009, pp. 69-74.
40. Schumann, U., and Konopka, P. "A simple estimate of the concentration field in a flight corridor," *Impact of Emissions from Aircraft and Spacecraft upon the Atmosphere. Proc. of an Intern. Sci. Colloquium, Köln (Cologne), Germany, April 18-20, 1994*. DLR-Mitt. 94-06, Köln, Germany, 1994, pp. 354-359.
41. Schumann, U., Konopka, P., Baumann, R., Busen, R., Gerz, T., Schlager, H., Schulte, P., and Volkert, H. "Estimate of diffusion parameters of aircraft exhaust plumes near the tropopause from nitric oxide and turbulence measurements," *J. Geophys. Res.* Vol. 100, 1995, pp. 14147-14162
42. Konopka, P. "Analytical Gaussian solutions for anisotropic diffusion in a linear shear flow," *J. Non-Equilib. Thermodyn.* Vol. 20, 1995, pp. 78-91
43. Schumann, U., Mayer, B., Gierens, K., Unterstrasser, S., Jessberger, P., Petzold, A., Voigt, C., and Gayet, J.-F. "Effective radius of ice particles in cirrus and contrails," *J. Atmos. Sci.* Vol. 68, No. 2, 2011, pp. 300-321, DOI: 10.1175/2010JAS3562.1.
44. Schumann, U., Mayer, B., Graf, K., Mannstein, H., and Meerkötter, R. "A parametric radiative forcing model for cirrus and contrail cirrus," *ESA Atmospheric Science Conference, Special Publication SP-676*. Barcelona, Spain, 7-11 September 2009, 2009, pp. 1-6.
45. Mayer, B., and Kylling, A. "The libRadtran software package for radiative transfer calculations: Description and examples of use," *Atmos. Chem. Phys.* Vol. 5, 2005, pp. 1855–1877, http://www.atmos-chem-phys.net/5/1855/2005/.
46. Petzold, A., Döpelheuer, A., Brock, C. A., and Schröder, F. "In situ observation and model calculations of black carbon emission by aircraft at cruise altitude," *J. Geophys. Res.* Vol. 104, 1999, pp. 22171-22181
47. Eyers, C. J., Addleton, D., Atkinson, K., Broomhead, M. J., Christou, R., Elliff, T., Falk, R., Gee, I., Lee, D. S., Marizy, C., Michot, S., Middel, J., Newton, P., Norman, P., Plohr, M., Raper, D., and Stanciou, N. "AERO2k Global Aviation Emissions Inventories for 2002 and 2025." QinetiQ for European Commission under Contract No. G4RD-CT-2000-00382, Farnborough, Hampshire, GU14 0LX, 2004.

48. Döpelheuer, A. "Anwendungsorientierte Vefahren zur Bestimmung von CO, HC und Ruß aus Luftfahrttriebwerken." Deutsches Zentrum für Luft- und Raumfahrt, FB 2002-10, Cologne, 2002, p. 109.
49. Voigt, C., Schumann, U., Jurkat, T., Schäuble, D., Schlager, H., Petzold, A., Gayet, J.-F., M. Krämer, Schneider, J., Borrmann, S., Schmale, J., Jessberger, P., Hamburger, T., Lichtenstern, M., Scheibe, M., Gourbeyre, C., Meyer, J., Kübbeler, M., Frey, W., Eichler, H., Butler, T., Lawrence, M. G., Holzäpfel, F., Arnold, F., Wendisch, M., Döpelheuer, A., Gottschaldt, K., Baumann, R., Zöger, M., Sölch, I., Rautenhaus, M., and Dörnbrack, A. "In-situ observations of young contrails – overview and selected results from the CONCERT campaign," *Atmos. Chem. Phys.* Vol. 10, 2010, pp. 9039-9056, doi:10.5194/acp-10-9039-2010.
50. Graf, K., Mannstein, H., Mayer, B., and Schumann, U. "Some evidence of aviation fingerprint in diurnal cycle of cirrus over the North Atlantic," *Proceedings of the 2nd International Conference on Transport, Atmosphere and Climate (TAC-2). 22-25 June 2009, DLR-Forschungsbericht 2010-10, Köln-Porz, Germany, ISSN 1434-8454*. Aachen and Maastricht, 2009, pp. 180-185.
51. Tompkins, A., Gierens, K., and Rädel, G. "Ice supersaturation in the ECMWF Integrated Forecast System," *Q. J. R. Meteorol. Soc.* Vol. 133, 2007, pp. 53–63, doi: 10.1002/qj.14.
52. Rädel, G., and Shine, K. P. "Evaluation of the use of radiosonde humidity data to predict the occurrence of persistent contrails," *Q. J. R. Meteorol. Soc.* Vol. 133, No. 627, 2007, pp. 1413-1423, doi: 10.1002/qj.128.
53. Lamquin, N., Gierens, K., Stubenrauch, C. J., and Chatterjee, R. "Evaluation of upper tropospheric humidity forecasts from ECMWF using AIRS and CALIPSO data," *Atmos. Chem. Phys.* Vol. 9, 2009, pp. 1779-1793, www.atmos-chem-phys.net/9/1779/2009/.
54. Wilkerson, J. T., Jacobson, M. Z., Malwitz, A., Balasubramanian, S., Wayson, R., Fleming, G., Naiman, A. D., and Lele, S. K. "Analysis of emission data from global commercial aviation: 2004 and 2006," *Atmos. Chem. Phys.* Vol. 10, 2010, pp. 6391-6408, doi:10.5194/acp-10-6391-2010.
55. Brasseur, G. P., and Gupta, M. "Impact of aviation on climate - research priorities," *Bull. Amer. Meteorol. Soc.* Vol. 91, No. April, 2010, pp. 461-463
56. Rap, A., Forster, P. M., Jones, A., Boucher, O., Haywood, J. M., Bellouin, N., and Leon, R. R. D. "Parameterization of contrails in the UK Met Office Climate Model," *J. Geophys. Res.* Vol. 115, 2010, p. D10205, doi:10.1029/2009JD012443.
57. Kärcher, B., Burkhardt, U., Ponater, M., and Frömming, C. "Importance of representing optical depth variability for estimates of global line-shaped contrail radiative forcing," *PNAS*, 2010, pp. 19181-19184, doi:10.1073/pnas.1005555107.
58. Minnis, P., D.F. Young, D.P. Garber, L. Nguyen, W.L. Smith Jr. and R. Palikonda. "Transformation of contrails into cirrus during SUCCESS," *Geophys. Res. Lett.* Vol. 25, 1998, pp. 1157-1160
59. EUROCONTROL. "Aircraft Performance Summary Tables for the Base of Aircraft Date (BADA), Revision 3.7." Vol. EEC Note No. 12/04, ACE-C-E2, European Organisation for the Safety of Air Navigation, Brétigny-sur-Orge, 2009.
60. Döpelheuer, A., and Lecht, M. "Influence of engine performance on emission characteristics," *Gas Turbine Engine Combustion, Emissions and Alternative Fuels*. RTO MP-14, ISBN 92-837-0009-0, paper 20, 1999, p. 11.
61. Gauss, M., Isaksen, I. S. A., Lee, D. S., and Søvde, O. A. "Impact of aircraft NO_x emissions on the atmosphere – tradeoffs to reduce the impact," *Atmos. Chem. Phys.* Vol. 6, 2006, pp. 1529–1548
62. Sausen, R., and Schumann, U. "Estimates of the climate response to aircraft CO_2 and NO_x-emission scenarios," *Climatic Change* Vol. 44, 2000, pp. 27 - 58
63. Ponater, M., Pechtl, S., Sausen, R., Schumann, U., and Hüttig, G. "Potential of the cryoplane technology to reduce aircraft climate impact: A state-of-the-art assessment," *Atmos. Env.* Vol. 40, 2006, pp. 6928–6944
64. Ponater, M. "Distinctive Efficacies of the components contributing to total aviation climate impact," *Proceedings of the 2nd International Conference on Transport, Atmosphere and Climate (TAC-2). 22-25 June 2009, DLR-Forschungsbericht 2010-10, Köln-Porz, Germany, ISSN 1434-8454*. Aachen, Germany, and Maastricht, The Netherlands, 2009, pp. 227-232.
65. Palikonda, R., P. Minnis, D.P. Duda and H. Mannstein. "Contrail coverage derived from 2001 AVHRR data over the continental United States of America and surrounding areas," *Meteorol. Z.* Vol. 14, 2005, pp. 525-536
66. Meyer, R., Mannstein, H., Meerkötter, R., Schumann, U., and Wendling, P. "Regional radiative forcing by line-shaped contrails derived from satellite data," *J. Geophys. Res.* Vol. 107, No. D10, 2002, pp. ACL 17-1 - ACL 17-15, 10.1029/2001jd000426.
67. Meyer, R., Buell, R., Leiter, C., Mannstein, H., Pechtl, S., Oki, T., and Wendling, P. "Contrail observations over Southern and Eastern Asia in NOAA/AVHRR data and comparisons to contrail simulations in a GCM," *Int. J. Rem. Sens.* Vol. 28, No. 9, 2007, pp. 2049-2069, doi:10.1080/01431160600641707.